Unraveling structural information of Turkevich synthesized plasmonic gold–silver bimetallic nanoparticles

DOI: 10.1002/ ((please add manuscript number))
Article type: Full paper

Unravelling Structural Information of Turkevich Synthesized Plasmonic Gold-silver Bimetallic Nanoparticles

*Natan Blommaerts, Hans Vanrompay, Silvia Nuti, Silvia Lenaerts, Sara Bals, Sammy W. Verbruggen**

N. Blommaerts, S. Nuti, Prof. S. Lenaerts, Prof. S.W. Verbruggen
Sustainable Energy, Air & Water Technology (DuEL), Department of Bioscience Engineering, University of Antwerp, Groenenborgerlaan 171, 2020 Antwerp, Belgium
E-mail: Sammy.Verbruggen@uantwerp.be
H. Vanrompay, S. Nuti, Prof. S. Bals
Electron Microscopy for Materials Science (EMAT), Department of Physics, University of Antwerp, Groenenborgerlaan 171, 2020 Antwerp, Belgium

Keywords: turkevich, surface plasmon resonance (SPR), electron tomography, FEM modeling, gold-silver bimetallic nanoparticles

Abstract

For the synthesis of gold-silver bimetallic nanoparticles, the Turkevich method has been the state-of-the-art method for several decades. It has been presumed that this procedure results in a homogeneous alloy, although this has been debatable for many years. In this work, it is shown that neither a full alloy, nor a perfect core-shell particle is formed but rather a core-shell-like particle with altering metal composition along the radial direction. In-depth wet-chemical experiments are performed in combination with advanced transmission electron microscopy, including EDX tomography, and Finite Element Method modeling to support the observations. From the electron tomography results, the core-shell structure could be clearly visualized and the spatial distribution of gold and silver atoms could be quantified. Theoretical simulations are performed to demonstrate that even though UV-Vis spectra show only one plasmon band, this still originates from core-shell type structures. The simulations also indicate that the core-shell morphology does not so much affect the location of the plasmon band, but mainly results in significant band broadening. Wet-chemistry experiments

provide the evidence that the synthesis pathway starts with gold enriched alloy cores, and later on in the synthesis mainly silver is incorporated to end up with a silver enriched alloy shell.

1. Introduction

The synthesis and characterization of metal nanoparticles has gained a lot of attention during the last decade due to their unique electronic, thermal, optical, and catalytic properties[1–8] leading to important technological applications such as plasmonic photo- and electrocatalysis[5,9–15], surface-enhanced Raman-spectroscopy[16–20], (bio)-sensors[21,22], and nano-electronic devices[21,23]. Bimetallic nanoparticles are of specific interest because of their versatility and tunability mainly for (photo)catalytic applications. Especially the gold-silver combination has been thoroughly investigated due to its optical surface plasmon resonance (SPR) absorbance that can be tuned over the entire visible range of the electromagnetic spectrum, merely depending on the composition of both metals.[2,13,14,24]

Various methods have been applied to synthesize Au-Ag bimetallic nanoparticles, of which the most widely used is the Turkevich method.[25] This method is based on the co-reduction of metal precursors in the presence of a stabilizing agent, usually sodium citrate, in boiling water. Most studies report on the formation of alloy nanoparticles[26–32], although some researchers have also indicated the possible formation of core-shell structures.[29,33] The assumption of a full alloy composition is mostly based on UV-Vis absorption data, that only show one single plasmon band in the visible light range.[29–32,34,35] Indeed, two separate plasmon bands are usually observed in the case of a core-shell structure.[27,35,36] Hereby, it is important to note that according to Mie Theory, the total extinction cross-section scales with the volume of the nanoparticles.[37] The observation of only one plasmon band in the UV-Vis spectrum therefore not excludes a core-shell structure, since such a morphology with a sufficiently thick shell also leads to a sole plasmon band. Other indirect evidence of alloy formation is provided by 2D energy-dispersive X-ray (EDX) projection images. However, 2D TEM projection images

of 3D objects can be very misleading and are not necessarily representative for the real 3D composition.[38]

In this work, we aim to accurately elucidate the real structure and synthesis pathway of gold-silver bimetallic nanoparticles, synthesized according to the universally applied Turkevich method, by analyzing samples taken at several time intervals during the synthesis. An experimental wet-chemical study is linked to both an advanced electron microscopy analysis, including EDX tomography, and extensive modeling. In this way a complete analysis is provided to once and for all unravel the structural enigma surrounding the Turkevich synthesis of gold-silver bimetallic nanoparticles.

2. Results and discussion

One of the most characteristic parameters of plasmonic nanoparticles is their surface plasmon resonance (SPR) absorption band in the UV-Vis spectrum. It is therefore the first and foremost criterion that hints at alloy formation or shaping of domains of different composition, *e.g.* core-shell structures.[29,34,36] It is a generally accepted idea that the appearance of a single plasmon band in the absorption spectrum hints at an alloy nanoparticle, while the appearance of two distinct plasmon bands indicates the co-existence of two separate metallic fractions (*e.g.* a core-shell structure). [27,35,36] Caution has to be taken, however, since one plasmon band can also indicate the appearance of a core-shell structure in which the shell is thick enough to eliminate the optical effect of the core's plasmon resonance, or that the nanoparticle consists of a gradually altering alloy composition as will be shown later. **Figure 1** shows the absorption spectrum of $Au_{0.5}Ag_{0.5}$ bimetallic nanoparticles after 30 min of synthesis time. Only one distinct plasmon band is visible in this spectrum, with a maximum around 470 nm, thus pointing at the formation of a full alloy nanoparticle at first glance. This is in line with earlier research on Au-Ag bimetallic nanoparticles.[29,31] As explained above, the information

provided by UV-Vis absorption spectroscopy is not sufficient for unambiguously identifying the type of nanostructure.

The size, shape and arrangement of the $Au_{0.5}$-$Ag_{0.5}$ nanoparticles synthesized under the same conditions, were investigated using high-angle annular dark-field scanning transmission electron microscopy (HAADF-STEM). HAADF-STEM projection images, visualized in **Figure 2**, illustrate that spherical nanoparticles were formed with a size of 50 ± 9 nm (size distribution histogram can be found in the supporting information Figure S1), as expected from previous work.[14,24] The advantage of HAADF-STEM is that the contrast can be correlated to the atomic number (Z) of the composing atoms. Since there is a significant difference in Z number between Au (79) and Ag (47), high intensities can hint at areas containing mostly Au, while darker areas can imply Ag rich regions. In contradiction to the expected alloy formation based on the UV-Vis spectrum, the results seem to indicate that rather than forming a full homogeneous alloy, the nanoparticles have formed a core-shell type of nanostructure. However, 2D projection images of a 3D object can be very misleading, and the presence of diffraction contrast complicates their quantitative interpretation. From Pd-Ag alloy nanoparticles, it is also known that silver has the tendency to segregate toward the surface of the particle.[39] In what follows, the formation mechanism of these $Au_{0.5}Ag_{0.5}$ bimetallic nanoparticles is therefore investigated in more detail. Samples were collected at several time intervals throughout the synthesis. The aliquots were rapidly cooled in ice to quench the reaction, and analyzed using UV-Vis spectroscopy, Spectroquant elemental analysis, electron tomography and EDX.

As can be observed from **Figure 3**, the solution starts to become slightly pink after 4 minutes of reaction, which is the typical color for gold nanoparticles suspended in water. As the reaction time increases, the color becomes darker and more orange, ending with a yellowish-orange solution which is a combination of the typical red color for gold and yellow color of silver nanoparticles. To analyze this color change in a quantitative manner, UV-Vis spectra

were taken for the same samples to identify the shape and location of the plasmon band (**Figure 4**). After 4 minutes, the first plasmon absorption band can be observed around 504 nm. This is close to the typical SPR band of gold, expected around 520 nm. This blue shift can be attributed to a smaller size of the seeds, or to the formation of an alloy with a low amount of silver present. As the reaction progresses, the plasmon band steadily blue shifts and increases in intensity as more particles are being formed and the silver content increases, as it is known that silver generates a stronger plasmonic response than gold. After 16 minutes, the synthesis seems to be completed since both the plasmon band position as well as the intensity remain unaltered.

To corroborate the results of the UV-Vis analysis, elemental analysis using the Spectroquant method was performed on the supernatant of the samples after centrifugation and removal of the precipitated bimetallic nanoparticles. This yields the concentration of gold ions left in solution after a given time of reaction, to enable the quantitative deduction of the amount of gold already incorporated in the nanoparticles. From the results in **Figure 5**, it is clear that the concentration of gold ions still in solution (blue curve) follows the same trend as for the plasmon band shift (red curve). There is a distinct lag on the plasmon band shift since the inflection point in the supernatant gold concentration is around 7 minutes whereas for the plasmon band shift this is around 11 minutes. This indicates that first mainly gold is incorporated in the particles, resulting in a plasmon band located over 500 nm which is close to that of pure gold nanoparticles. This is in agreement with literature reports stating that the difference in redox potential between gold and silver leads to a sequential reduction in which gold nuclei are preferentially formed.[34,40] After 10 minutes, there is almost no gold left in the solution and it is assumed that most of the gold ions are incorporated in the particles at this point. Looking at the curve of the plasmon band after 10 min, the wavelength shifted to 495 which is still a small shift, indicating that only a small fraction of silver ions is incorporated in the particles at this point. If gold and silver were incorporated in an equal amount, then after

10 minutes all the silver would have been included as well. Consequently, the plasmon band would have reached its final wavelength (disregarding minor shifts due to size and shape contributions). Since this is not the case, it is concluded that the silver is mainly incorporated at a later stage of the synthesis.

To complement these wet-chemical results, HAADF-STEM tomography and EDX mapping were performed on five different time steps (4, 7, 10, 13, 16 min). In the first column of **Figure 6**, single HAADF-STEM projection images of different nanoparticles acquired after 4, 7, 10, 13 and 16 minutes of synthesis are displayed. In the second and third column respectively, the EDX maps of Au (red) and Ag (green) are shown. The last column displays the superposition of both maps. Comparing the combined EDX maps for the different time steps indicates that although the nanoparticles apparently form an alloy at the beginning of the synthesis, they steadily develop a silver-enriched shell across the nanoparticle's surface. From Figure 6c it can be seen that even after one EDX map, the Ag shell forms clusters along the nanoparticle's surface. At later stages of the reaction, as the formation of the shell continues, this effect becomes less pronounced. This shows that initially the Ag enriched shell is highly unstable under long electron beam exposure, making a quantitative 3D EDX analysis of the earlier stages unfeasible. Therefore HAADF-STEM tomography was performed on all different stages of the synthesis procedure. While HAADF-STEM tomography does not lead to any quantitative information concerning the chemical composition of the nanoparticle, it can offer a qualitative picture, since the atomic numbers of Au and Ag are very different as discussed above. 3D renderings of the reconstruction and the corresponding central orthoslices of the same nanoparticles are shown in supporting information Figure S2. By comparing different reaction stages, it becomes obvious that the particle formation starts off as a homogeneous alloy but gradually gains the characteristics of a core-shell nanostructure. After 10 minutes of synthesis the first signs of a shell are visible in the HAADF-STEM reconstruction. As the synthesis continues, the shell further grows until it is almost 5 nm thick.

Given the increased stability of the final state of the nanoparticle, EDX tomography was performed on the 16 min sample using the ζ-method[41]. This method consists of a synergistic combination of HAADF-STEM - and EDX tomography for which each voxel of the final reconstruction contains a distribution of the different elements of the nanoparticle, in this case Au and Ag. In this manner, not only qualitative but also quantitative information concerning the 3D composition of the final state is retrieved.[41,42] In **Figure 7**a, a 3D rendering of the investigated particle is presented. In the central orthoslice through the reconstruction (Figure 7b), a clear core-shell morphology is visible because of the large difference in gray value between their relative compositions. Orthoslices through the Au and Ag signal of the corresponding EDX tomography reconstruction confirm that the core contains a higher amount of Au, whereas the shell primarily contains Ag (see supporting information Figure S3 for ZX orthoslices and Figure S4 for ZY orthoslices). This agrees with the HAADF-STEM reconstructions for which the core consistently showed a higher intensity than the shell. From the HAADF-STEM reconstruction a mask was derived for both the core and the shell through histogram-based segmentation. By multiplying these masks with the Au and Ag reconstructions, it is possible to separate the contributions of both regions for the Au and Ag signal. It was found that on average the core contains 82 ± 3% Au and 18 ± 2% Ag, whereas the shell approximately consists of 35 ± 4% Au and 65 ± 5% Ag. This agrees with the central line profile through the EDX reconstruction as presented in **Figure 8**. This inhomogeneous elemental distribution could explain the strange behavior with regard to Vegard's law[43] that was recently observed by Prymak et al.[40] They showed that negative deviations from Vegard's law were found for wet-chemically synthesized Au-Ag bimetallic nanoparticles whereas laser-ablated nanoparticles, synthesized according to Neumeister et al.[44], followed the law perfectly. This negative deviation was found highest for a 50:50 composition as shown by Grasmik et al.[45]

Even though the EDX tomography results prove that the nanoparticles show clear characteristics of a core-shell nanostructure, the UV-Vis spectrum in Figure 1 still shows only one plasmon band, which is indicative of a full alloy. To understand the nature of this single plasmon absorption band, theoretical calculations based on FEM modeling were performed. The model was constructed as a single 3D nanoparticle of 50 nm in diameter in which the alloy composition is predefined to vary continuously in the radial direction according to the line profile in Figure 8, with smooth transitions between layers of different compositions. The complex dielectric functions for predefined alloy compositions were taken from literature[46] and incorporated in the model. An example of the radius dependent refractive index data based on the alloy composition is shown in Figure S5. To reduce the calculation time, a finite number of maximum five different alloy compositions with a smooth transition was chosen and compared with the case for only two or three different alloy compositions (see Supporting info Figure S5). Intermittent non-geometrical spherical domains were meshed using a custom setting in COMSOL Multiphysics with a maximum element size of 1 nm to improve the meshing quality within the alloy nanoparticles and all the rest of the physical domains had extra fine meshing size with an average element mesh quality of 0.7 (Figure S6). Water was taken as the surrounding medium and a plane wave polarized in the Z-axis direction, and propagating along the X-axis direction was used for solving the scattered field of Maxwell's wave equations in a wavelength domain study. The incident polarized plane wave with a magnitude of E_0 = 1 V/m, was swept over a wide range from 300 to 800 nm to calculate absorption data of the bimetallic nanoparticle.

The results of the simulations are plotted in **Figure 9**, compared with the experimental data and simulated data of a perfect 50:50 alloy. It is interesting to note how the plasmon band position for the experimental and for the simulated data of a perfect 50:50 Au-Ag alloy almost match exactly, however, a clear band broadening is observed in the experimental absorption curve in comparison with the simulated curve, that is usually attributed to a broad particle size

distribution.[47] It seems that the shell is not necessarily too thick to eliminate the contribution of the core to the overall plasmonic behavior. Since the nanoparticle consists of a gradually altering alloy composition with no abrupt transition from core to shell the plasmon band position is determined by the total composition which is still 50:50. For the simulations based on a core-shell particle with gradually altering alloy composition, in the case of two and three compositions the plasmon band is significantly blue-shifted in comparison with the experimental data, and the band has broadened significantly. The blue-shift can be explained by the fact that in this case, the plasmon band position is mainly dominated by the 80% silver at the outside of the particle which is assumed too thick in this case. By approaching the actual compositional variation as per the line scan in Figure 8 by incorporating up to five different alloy compositions in the shell region, the plasmon band position almost perfectly coincides with the experimental data. The band also shows significant broadening alike the experimental spectrum, which was not the case when assuming a complete and homogeneous alloy nanoparticle. We assume that by accounting for variations in shape and particle size, band broadening would become even more pronounced and the experimental extinction spectrum could be matched even better.

3. Conclusion

In this work, we have provided evidence that the Turkevich synthesis of bimetallic $Au_{0.5}Ag_{0.5}$ nanoparticles does not result in a full and homogeneous alloy, as has often been presumed based on the single absorption band in the UV-Vis spectrum. Rather a core-shell-like nanostructure is formed in which the alloy composition changes gradually in the radial direction. The shell is enriched in silver (on average 65% silver and 35% gold), whereas the core is enriched in gold (on average 82% gold and 18% silver). Wet-chemical experiments provide the evidence that the synthesis pathway starts with gold (enriched) seeds, and later on in the synthesis, silver is incorporated to end up with a silver enriched shell. EDX tomography clearly showed the core-shell structure, providing the spatial composition of silver and gold

atoms. Based on these data it could be concluded that both the shell and the core consist of alloys with gradually altering compositions. Using the results from EDX tomography as input data for theoretical simulations, we could prove that even though the UV-Vis spectrum shows only one plasmon band, this still originates from a core-shell-like nanostructure. According to the simulations the main difference between a perfect alloy and the core-shell-like alloy nanoparticle is not the position of the plasmon band, but mainly the band broadening that becomes more pronounced.

4. Experimental Section

$Au_{0.5}Ag_{0.5}$ bimetallic nanoparticle synthesis: The following chemicals were purchased and used as received: sodium citrate (Chem-lab); silver nitrate (Sigma-Aldrich, >99.0%); chloroauric acid (Sigma-Aldrich, >99.9%). The synthesis of $Au_{0.5}Ag_{0.5}$ bimetallic particles was based on the Turkevich synthesis.[25] Briefly, it started by adding a $AgNO_3$ solution (500 μL, 0.01 M) in deionized water (98mL) under vigorous stirring. Then the solution was heated until right before boiling, at this point $HAuCl_4$ (500 μL, 0.01 M) was added. In this way, possible complexation of Ag^+ ions with Cl^- ions is strongly reduced. When the solution started to boil, an aqueous sodium citrate solution (1 mL, 1 wt%) was added as reducing and stabilizing agent and the solution was left boiling for 30 min until a clear orange solution was obtained. During the reaction, aliquots were taken at different reaction times (2, 4, 7, 10, 13, 16, 20, 25, 30 min) for analysis.

Characterization: UV-Vis absorption spectra of colloidal Au-Ag bimetallic nanoparticles were recorded with a Shimadzu UV-Vis 2501PC double beam spectrophotometer. Three consecutive scans were averaged in the wavelength range of 400-800 nm at a resolution of 0.2 nm to accurately locate the SPR band position. Spectroquant (NOVA 60, Merck) analysis was performed to quantitatively determine the Au concentration in colloidal suspension using a standard gold test kit (114821). The HAADF-STEM electron tomography (ET) experiments were performed using a Thermo Fischer Tecnai Osiris microscope operated at 200 kV. The

probe convergence semi angle equalled 16 mrad and a camera length of 115 mm was selected, corresponding to inner and outer collection semi angles of respectively 80 mrad and 240 mrad. A Fischione tomography holder (model 2020) was used to acquire the HAADF-STEM tilt series over a tilt range of ±75° with a 3° increment. After the acquisition, the images were aligned with respect to each other using a cross correlation. The outcome was used as an input for the ASTRA toolbox implementation[48] of the Expectation-Maximization algorithm (EM)[49], resulting in a 3D reconstruction of the morphology of the nanoparticle. To retrieve the metal composition of the nanoparticles, EDX tomography was performed on the Thermo Fischer Tecnai Osiris microscope as well operated under the same settings. The EDX tilt series were acquired over an angular range of ±70° with a tilt increment of 10° using the Super-X detection system and the same holder. Afterwards the so-called "ζ-factor" was used to quantitatively reconstruct the 3D composition of nanomaterials.[41,42]

Theoretical simulations: Finite Element Method (FEM) modeling was used to solve for Maxwell's electromagnetic differential equations in three dimensions. FEM can be used to solve for periodic structures and arbitrary shapes and has the highly useful advantage that it allows for the coupling of fields and physical quantities. In this work, the wave optics module of COMSOL Multiphysics® program was used to solve Maxwell's wave equations with respect to the scattered electric field. For more information the reader is referred to Asapu *et al.*[16] Details about the mesh geometry can be found in the supporting information.

Supporting Information

Supporting Information is available from the Wiley Online Library or from the author.

Acknowledgements

All authors wish to thank the University of Antwerp for financial support (GOA). The authors thank the Research Foundation – Flanders for a predoctoral fellowship (FWO grant 1S32617N) and project funding (FWO grant: G.0369.15N and G.0381.16N)

Conflict of Interest

The authors declare no conflict of interest.

Received:
Revised:
Published online:

References

[1] N. Claes, R. Asapu, N. Blommaerts, S. W. Verbruggen, S. Lenaerts, S. Bals, *Nanoscale* **2018**, *10*, 9186.

[2] L. M. Liz-Marzán, *Langmuir* **2006**, *22*, 32.

[3] S. W. Verbruggen, *J. Photochem. Photobiol. C Photochem. Rev.* **2015**, *24*, 64.

[4] S. Sarina, H. Y. Zhu, S. Sarina, H. Zhu, E. Jaatinen, Q. Xiao, H. Liu, J. Jia, C. Chen, *J. Am. Chem. Soc.* **2013**, *135*, 5793−5801.

[5] R. Asapu, N. Claes, S. Bals, S. Denys, C. Detavernier, S. Lenaerts, S. W. Verbruggen, *Appl. Catal. B Environ.* **2017**, *200*, 31.

[6] M. S. Shore, J. Wang, A. C. Johnston-Peck, A. L. Oldenburg, J. B. Tracy, *Small* **2011**, *7*, 230.

[7] A. Csaki, F. Jahn, I. Latka, T. Henkel, D. Malsch, T. Schneider, K. Schröder, K. Schuster, A. Schwuchow, R. Spittel, D. Zopf, W. Fritzsche, *Small* **2010**, *6*, 2584.

[8] Y. Wang, A. B. Serrano, K. Sentosun, S. Bals, L. M. Liz-Marzán, *Small* **2015**, *11*, 4314.

[9] F. Su, T. Wang, R. Lv, J. Zhang, P. Zhang, J. Lu, J. Gong, *Nanoscale* **2013**, *5*, 9001.

[10] S. Mourdikoudis, M. Chirea, D. Zanaga, T. Altantzis, M. Mitrakas, S. Bals, L. M. Liz-Marzán, J. Pérez-Juste, I. Pastoriza-Santos, *Nanoscale* **2015**, *7*, 8739.

[11] X.-Y. Yang, L.-H. Chen, Y. Li, J. C. Rooke, C. Sanchez, B.-L. Su, *Chem. Soc. Rev.* **2017**, *46*, 481.

[12] N. Blommaerts, R. Asapu, N. Claes, S. Bals, S. Lenaerts, S. W. Verbruggen, *Chem. Eng. J.* **2017**, *316*, 850.

[13] S. W. Verbruggen, M. Keulemans, B. Goris, N. Blommaerts, S. Bals, J. A. Martens, S. Lenaerts, *Appl. Catal. B Environ.* **2016**, *188*, 147.

[14] S. W. Verbruggen, M. Keulemans, M. Filippousi, D. Flahaut, G. Van Tendeloo, S. Lacombe, J. a. Martens, S. Lenaerts, *Appl. Catal. B Environ.* **2014**, *156–157*, 116.

[15] W.-S. Wang, H. Du, R.-X. Wang, T. Wen, A.-W. Xu, *Nanoscale* **2013**, *5*, 3315.

[16] R. Asapu, R.-G. Ciocarlan, N. Claes, N. Blommaerts, M. Minjauw, T. Ahmad, J. Dendooven, P. Cool, S. Bals, S. Denys, C. Detavernier, S. Lenaerts, S. W. Verbruggen, *ACS Appl. Mater. Interfaces* **2017**, *9*, 41577.

[17] S. Pande, S. K. Ghosh, S. Praharaj, S. Panigrahi, S. Basu, S. Jana, A. Pal, T. Tsukuda, T. Pal, *J. Phys. Chem. C* **2007**, *111*, 10806.

[18] Y. Cui, B. Ren, J.-L. Yao, R.-A. Gu, Z.-Q. Tian, *J. Phys. Chem. B* **2006**, *110*, 4002.

[19] G. Zheng, S. de Marchi, V. López-Puente, K. Sentosun, L. Polavarapu, I. Pérez-Juste, E. H. Hill, S. Bals, L. M. Liz-Marzán, I. Pastoriza-Santos, J. Pérez-Juste, *Small* **2016**, *12*, 3935.

[20] R. Asapu, N. Claes, R.-G. Ciocarlan, M. Minjauw, C. Detavernier, P. Cool, S. Bals, S. W. Verbruggen, *ACS Appl. Nano Mater.* **2019**, DOI 10.1021/acsanm.9b00485.

[21] S. Karmakar, S. Kumar, R. Rinaldi, G. Maruccio, *J. Phys. Conf. Ser.* **2011**, *292*, 012002.

[22] S. A. Zynio, A. V. Samoylov, E. R. Surovtseva, V. M. Mirsky, Y. M. Shirshov, *Sensors* **2002**, *2*, 62.

[23] A. Kamyshny, S. Magdassi, *Small* **2014**, *10*, 3515.

[24] S. W. Verbruggen, M. Keulemans, J. A. Martens, S. Lenaerts, *J. Phys. Chem. C* **2013**, *117*, 19142.

[25] J. Turkevich, P. C. Stevenson, J. Hillier, *J. Phys. Chem.* **1953**, *57*, 670.

[26] A. Pal, S. Shah, V. Kulkarni, R. S. R. Murthy, S. Devi, *Mater. Chem. Phys.* **2009**, *113*, 276.

[27] T.-W. Liao, A. Yadav, K.-J. Hu, J. van der Tol, S. Cosentino, F. D'Acapito, R. E. Palmer, C. Lenardi, R. Ferrando, D. Grandjean, P. Lievens, *Nanoscale* **2018**, *10*, 6684.

[28] Y. Yang, X. Gong, H. Zeng, L. Zhang, X. Zhang, C. Zou, S. Huang, *J. Phys. Chem. C* **2010**, *114*, 256.

[29] S. Link, Z. L. Wang, *J. Phys. Chem. B* **1999**, *103*, 3529.

[30] M. P. Mallin, C. J. Murphy, *Nano Lett.* **2002**, *2*, 1235.

[31] J. F. Sánchez-Ramírez, U. Pal, L. Nolasco-Hernández, J. Mendoza-Álvarez, J. A. Pescador-Rojas, *J. Nanomater.* **2008**, *2008*, 9.

[32] M. A. Uppal, M. B. Ewing, I. P. Parkin, *Eur. J. Inorg. Chem.* **2011**, 4534.

[33] K. Kim, K. L. Kim, J.-Y. Choi, H. B. Lee, K. S. Shin, *J. Phys. Chem. C* **2010**, *114*, 3448.

[34] T. Li, B. Albee, M. Alemayehu, R. Diaz, L. Ingham, S. Kamal, M. Rodriguez, S. Whaley Bishnoi, *Anal. Bioanal. Chem.* **2010**, *398*, 689.

[35] C. M. Gonzalez, Y. Liu, J. C. Scaiano, *J. Phys. Chem. C* **2009**, *113*, 11861.

[36] L. Lu, G. Burkey, I. Halaciuga, D. V Goia, *J. Colloid Interface Sci.* **2013**, *392*, 90.

[37] G. Mie, *Ann. Phys.* **1908**, *330*, 377.

[38] H. Vanrompay, E. Bladt, W. Albrecht, A. Béché, M. Zakhozheva, A. Sánchez-Iglesias, L. M. Liz-Marzán, S. Bals, *Nanoscale* **2018**, *10*, 22792.

[39] O. M. Løvvik, S. M. Opalka, *Surf. Sci.* **2008**, *602*, 2840.

[40] O. Prymak, J. Jakobi, C. Rehbock, M. Epple, S. Barcikowski, *Mater. Chem. Phys.* **2018**, *207*, 442.

[41] D. Zanaga, T. Altantzis, J. Sanctorum, B. Freitag, S. Bals, *Ultramicroscopy* **2016**, *164*, 11.

[42] D. Zanaga, T. Altantzis, L. Polavarapu, L. M. Liz-Marzán, B. Freitag, S. Bals, *Part. Part. Syst. Charact.* **2016**, *33*, 396.

[43] L. Vegard, *Zeitschrift für Phys.* **1921**, *5*, 17.

[44] A. Neumeister, J. Jakobi, C. Rehbock, J. Moysig, S. Barcikowski, *Phys. Chem. Chem. Phys.* **2014**, *16*, 23671.

[45] V. Grasmik, C. Rurainsky, K. Loza, M. V Evers, O. Prymak, M. Heggen, K. Tschulik, M. Epple, *Chem. – A Eur. J.* **2018**, *24*, 9051.

[46] D. Rioux, S. Vallières, S. Besner, P. Muñoz, E. Mazur, M. Meunier, *Adv. Opt. Mater.* **2014**, *2*, 176.

[47] C. J. Addison, A. G. Brolo, *Langmuir* **2006**, *22*, 8696.

[48] W. van Aarle, W. J. Palenstijn, J. De Beenhouwer, T. Altantzis, S. Bals, K. J. Batenburg, J. Sijbers, *Ultramicroscopy* **2015**, *157*, 35.

[49] T. K. Moon, *IEEE Signal Process. Mag.* **1996**, *13*, 47.

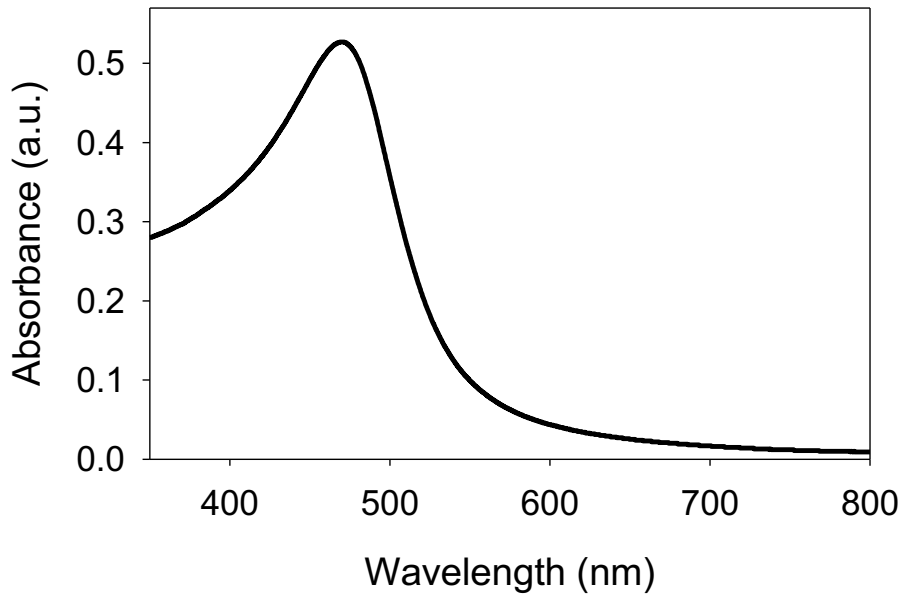

Figure 1. UV-Vis absorption spectrum of $Au_{0.5}Ag_{0.5}$ bimetallic nanoparticles after 30 min of synthesis.

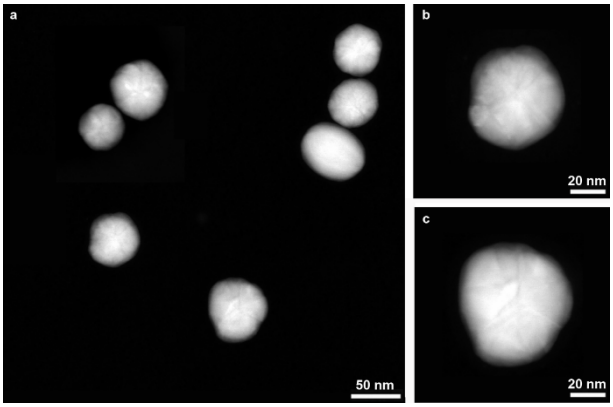

Figure 2. a-c) HAADF-STEM images of spherical $Au_{0.5}Ag_{0.5}$ bimetallic nanoparticles with an average size around 50 nm.

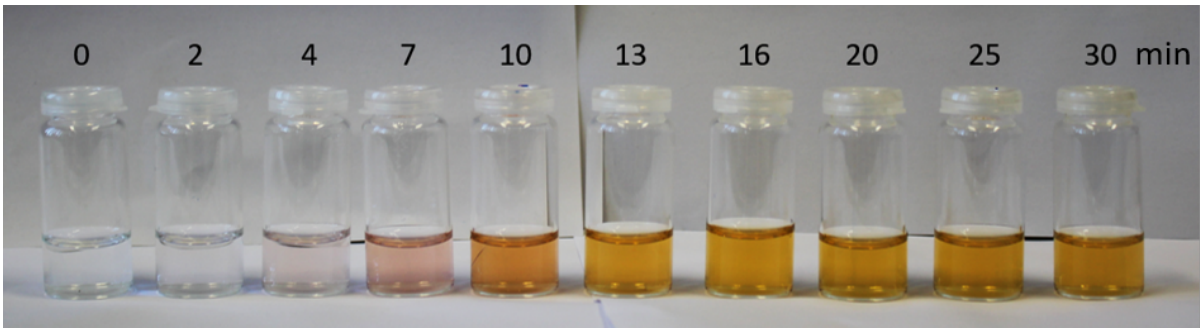

Figure 3. Pictures of the colloidal particles during synthesis. The numbers indicate the reaction time (min) at which the sample was taken. The starting point of the synthesis is the moment when sodium citrate is added to the boiling solution.

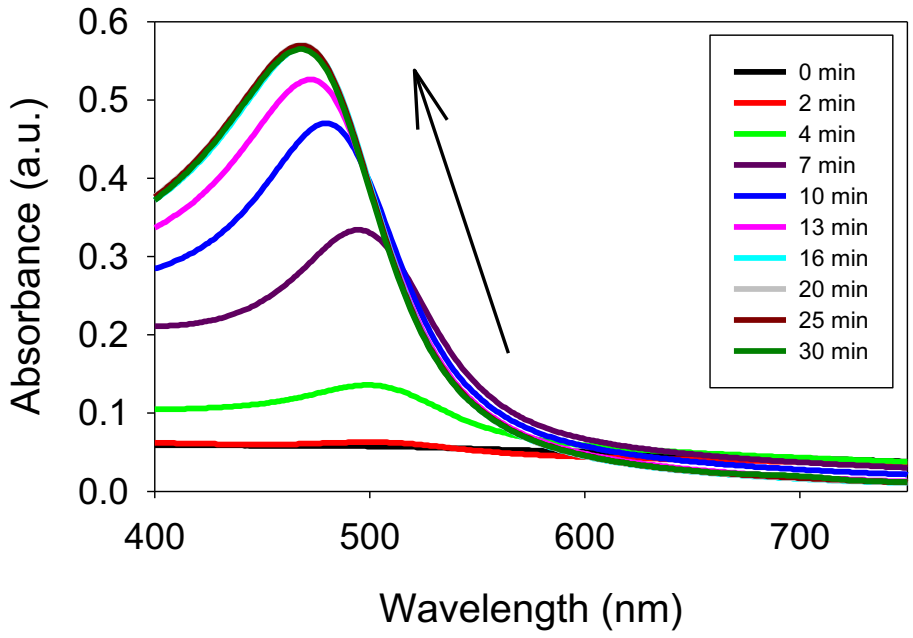

Figure 4. UV-Vis spectrum of $Au_{0.5}Ag_{0.5}$ nanoparticles at different reaction times.

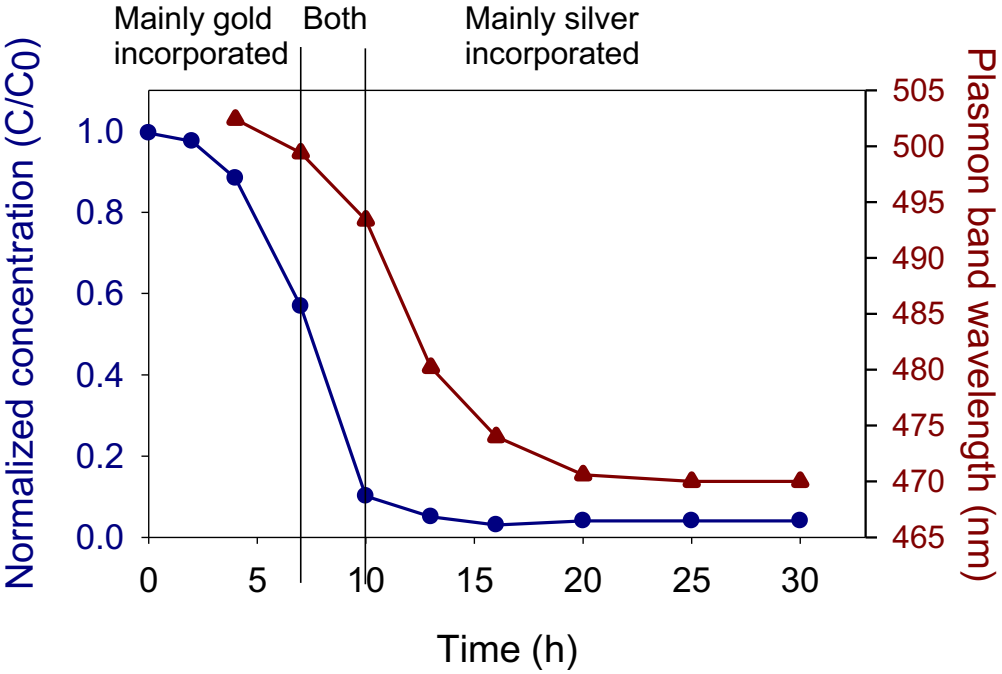

Figure 5. Plasmon absorption band position as a function of synthesis time (red ▲) and Spectroquant analysis for gold on the supernatant (blue ●), after centrifugation of samples taken during the synthesis of $Au_{0.5}Ag_{0.5}$ nanoparticles. The concentration at each time point is normalized toward the starting Au^{+} concentration.

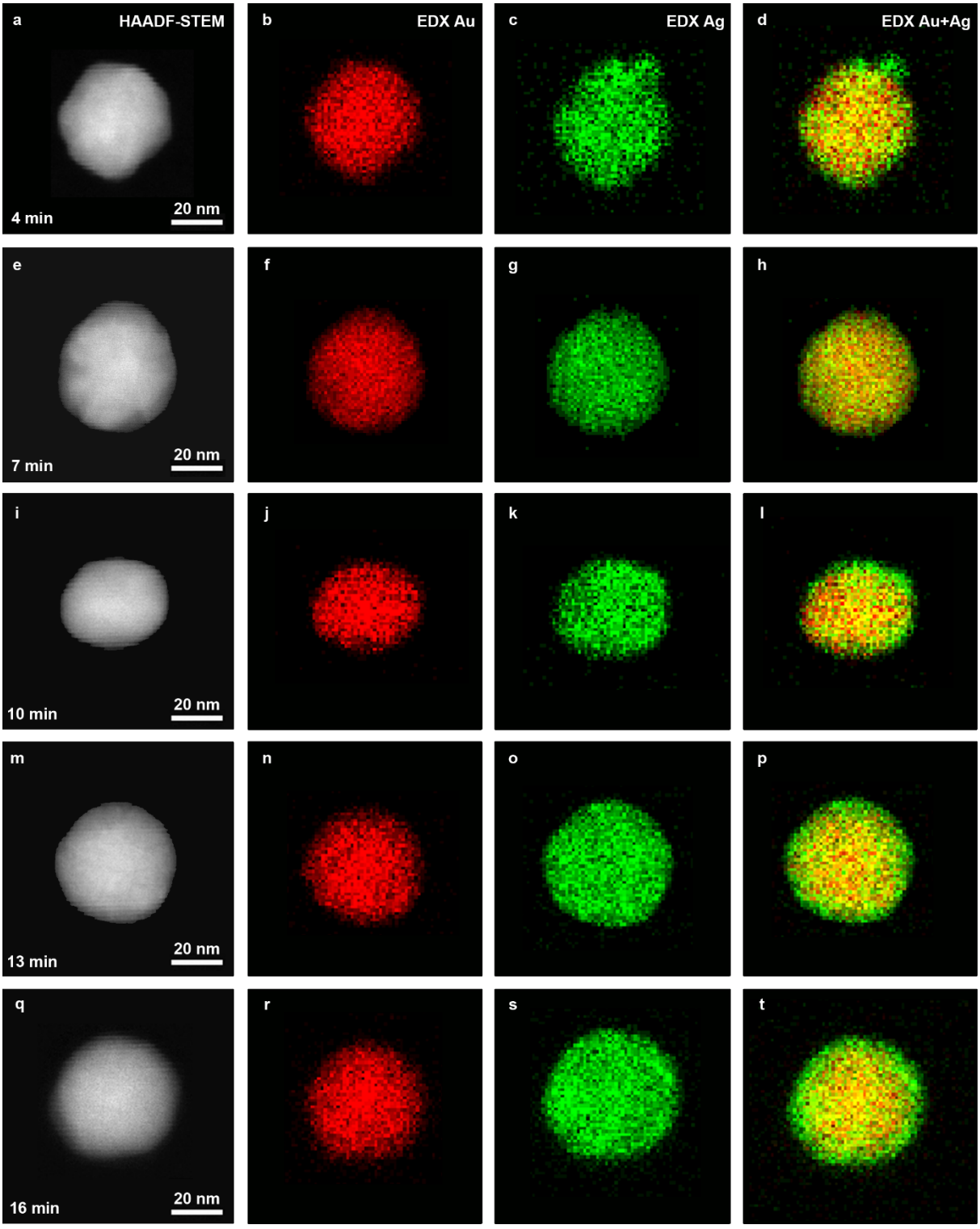

Figure 6. HAADF-STEM and net count EDX-maps of different nanoparticles sampled at intermediate times during the synthesis procedure.

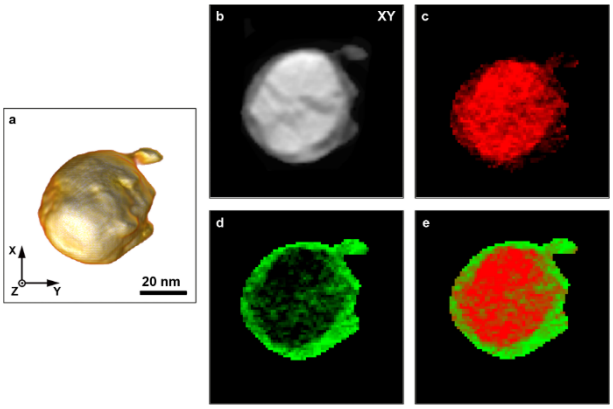

Figure 7. a-b) 3D rendering and a central XY orthoslice of the HAADF-STEM tomographic reconstruction of a nanoparticle obtained after 16 min of synthesis. c-d) Central XY orthoslices through the corresponding EDX tomography of the Ag and Au signal. e) Superposition of the Ag and Au signal.

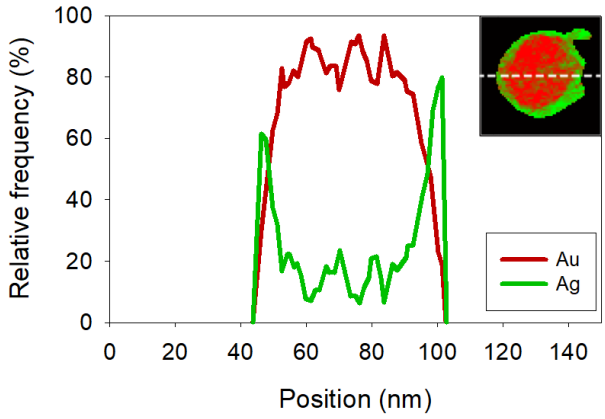

Figure 8. Central line profile through the XY orthoslice (as indicated in the figure's inset), revealing the 80% Au- 20% Ag composition of the core and the 35% Au - 65% Ag composition of the shell.

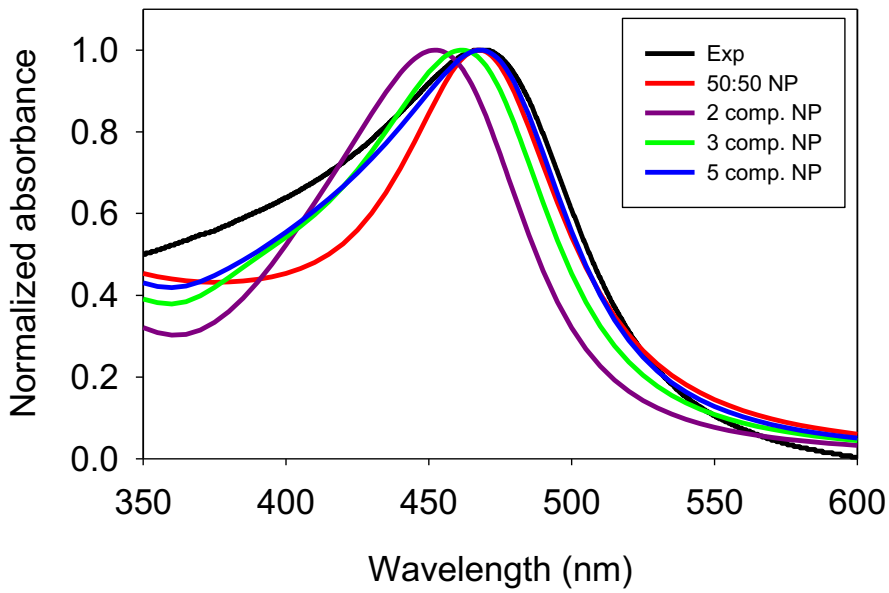

Figure 9. Comparison between experimental (black solid line) and simulated UV-Vis spectra of $Au_{0.5}Ag_{0.5}$ nanoparticles. The simulations are performed for a perfect 50:50 alloy (red line), and a series of core-shell type of nanoparticles including a particle consisting of two (purple line), three (green line), and five (blue line) gradually varying alloy compositions.

Table of Contents Entry

Turkevich synthesis of Au-Ag bimetallic nanoparticles results in core-shell-like nanostructures with a gradually varying alloy composition in the radial direction. A complete analysis including wet-chemical experiments, advanced electron microscopy and extensive FEM modeling is performed to reveal that the core is enriched in gold (80% Au) and the shell is enriched in silver (65% Ag).

N. Blommaerts, H. Vanrompay, S. Nuti, S. Lenaerts, S. Bals, S. W. Verbruggen*

Unravelling Structural Information of Turkevich Synthesized Plasmonic Gold-silver Bimetallic Nanoparticles

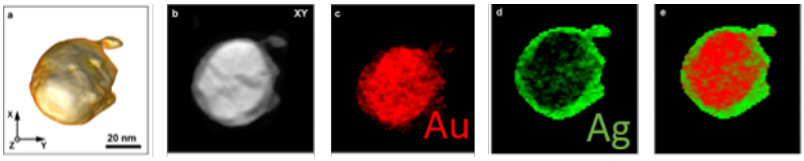

Keywords

Gold-Silver; Turkevich; Nanoparticle; Alloy; Core-Shell; Plasmon; Electron Tomography